

Annual Review of Physical Chemistry
**Electron Transfer from
 Semiconductor Nanocrystals
 to Redox Enzymes**

James K. Utterback,^{1,2} Jesse L. Ruzicka,¹
 Helena R. Keller,³ Lauren M. Pellows,¹
 and Gordana Dukovic¹

¹Department of Chemistry, University of Colorado Boulder, Boulder, Colorado 80309, USA; email: jesse.ruzicka@colorado.edu, lauren.pellows@colorado.edu, gordana.dukovic@colorado.edu

²Current affiliation: Department of Chemistry, University of California, Berkeley, California 94720, USA; email: james.utterback@berkeley.edu

³Materials Science and Engineering Program, University of Colorado Boulder, Boulder, Colorado 80309, USA; email: helena.keller@colorado.edu

Annu. Rev. Phys. Chem. 2020. 71:335–59

First published as a Review in Advance on
 February 25, 2020

The *Annual Review of Physical Chemistry* is online at
physchem.annualreviews.org

<https://doi.org/10.1146/annurev-physchem-050317-014232>

Copyright © 2020 by Annual Reviews.
 All rights reserved

Keywords

charge transfer, nanocrystal, redox enzyme, biohybrid, photochemistry, time-resolved spectroscopy

Abstract

This review summarizes progress in understanding electron transfer from photoexcited nanocrystals to redox enzymes. The combination of the light-harvesting properties of nanocrystals and the catalytic properties of redox enzymes has emerged as a versatile platform to drive a variety of enzyme-catalyzed reactions with light. Transfer of a photoexcited charge from a nanocrystal to an enzyme is a critical first step for these reactions. This process has been studied in depth in systems that combine Cd-chalcogenide nanocrystals with hydrogenases. The two components can be assembled in close proximity to enable direct interfacial electron transfer or integrated with redox mediators to transport charges. Time-resolved spectroscopy and kinetic modeling have been used to measure the rates and efficiencies of the electron transfer. Electron transfer has been described within the framework of Marcus theory, providing insights into the factors that can be used to control the photochemical activity of these biohybrid systems. The range of potential applications and reactions that can be achieved using nanocrystal-enzyme systems is expanding, and numerous fundamental and practical questions remain to be addressed.

ANNUAL
 REVIEWS **CONNECT**

www.annualreviews.org

- Download figures
- Navigate cited references
- Keyword search
- Explore related articles
- Share via email or social media

1. INTRODUCTION

ET: electron transfer

Redox enzyme:

a protein that catalyzes reduction and oxidation reactions

Nanocrystal (NC):

a nanoscale crystalline particle with dimensions on the order of the exciton Bohr radius of the corresponding bulk semiconductor

Quantum dot (QD):

a spherically shaped semiconductor nanocrystal

Nanorod (NR):

a cylindrically shaped semiconductor nanocrystal

Redox mediator:

a chemical species that shuttles charge carriers from donor to acceptor

Nature has evolved efficient and selective electrocatalysts in the form of oxidoreductases: enzymes that can catalyze a wide variety of multielectron redox reactions with remarkable selectivity and low overpotentials, leading to little energy waste (1, 2). The study of oxidoreductase structure and function has the potential to advance the catalysis of a wide range of reactions that may otherwise be difficult, energy-intensive, or both to achieve with artificial catalysts (2). Oxidoreductase catalysis requires externally supplied redox equivalents (electrons or holes). In vivo electron transfer (ET) mechanisms rely on diffusion-limited interactions with biological cofactors (3, 4), thereby making the charge-transfer steps relatively slow, complex, and sometimes rate-limiting for enzyme catalysis (5). Redox enzymes stabilize intermediate oxidation states, enabling multielectron catalysis when electron flux is low (6). To enhance control over electron delivery to redox enzymes, systems that integrate enzymes with electrode surfaces or photosensitizers were developed as early as the 1960s (1, 7–10).

A variety of nanomaterials have been used as photosensitizers to drive enzymatic reactions with light, including various Cd-chalcogenide nanocrystals (NCs) (5, 11–32), PbS quantum dots (QDs) (33), carbon dots (34, 35), carbon nitride nanorods (NRs) (36), and both bare and dye-sensitized TiO₂ (37–44). Many of these systems have targeted solar-to-fuel conversion (1, 10, 19, 45–51), primarily H₂ production (14, 16, 17, 21, 30, 31, 34, 37–39, 42), but efforts have expanded to pursue a wide variety of reactions, such as N₂ fixation (25), carbon-carbon (C–C) bond formation (24), CO₂ reduction to CO (19, 40, 44), biological cofactor regeneration (26), reduction of fumarate to succinate (34), reduction of aldehydes to alcohols (26), stereoselective chemistry (18, 36, 41, 52), *trans*-specific reduction of an activated alkene bond (35), phosphorylation of guanosine monophosphate (23), dehalogenation (43), and monooxygenation of myristic acid (11), as well as photoelectrochemical sensing of sugars (15, 29, 33), superoxides (13), sulfites (27), lactate (12), and nitrates (12) on NC-modified electrodes.

Here, we focus on the use of photoexcited NCs of Cd-chalcogenides (CdS, CdSe, CdTe, and related heterostructures) as charge donors for enzyme catalysis (5, 11–32, 52). NCs are an attractive choice for this purpose for several reasons. They are excellent light absorbers due to their large extinction coefficients (53). They can be suspended in colloidal solution or deposited as solid thin films (54, 55). Many of their key properties are readily tunable—most notably their size, shape, energy-level structure, redox potentials, and surface chemistry (53, 54, 56–58). Additionally, quantum confinement and large surface area-to-volume ratios in NCs can lead to increased electronic coupling with charge acceptors, thereby increasing the rate of charge transfer and improving its efficiency (59–61). The NC properties can be tuned to control not only the binding interactions with the enzyme but also the factors that govern transfer of photoexcited charges from the NC to the enzyme.

In light-driven reactions of Cd-chalcogenide NC–enzyme biohybrids, the NC acts as the light harvester, while the enzyme acts as the cocatalyst. Light absorption by the NC produces photoexcited electrons and holes. In photoreduction reactions, shown in **Figure 1**, the electron transfers to the enzyme while the NC is returned to the neutral state through hole scavenging by a sacrificial electron donor molecule or an electrode. In the case of enzymatic oxidation, it is the photoexcited hole that transfers to the enzyme while the electron is scavenged sacrificially. Charge transfer can occur directly, when the enzyme is bound closely to the NC, or indirectly, when redox mediators shuttle charges between the NC and enzyme. Within the enzyme, the charge is transported from the injection site to the active site, where it participates in the catalytic cycle. The photochemical reactions usually involve multiple electrons, and this cycle repeats in a series of light-driven charge-transfer events and redox reactions at the enzyme active site, leading to the formation of the photochemical product.

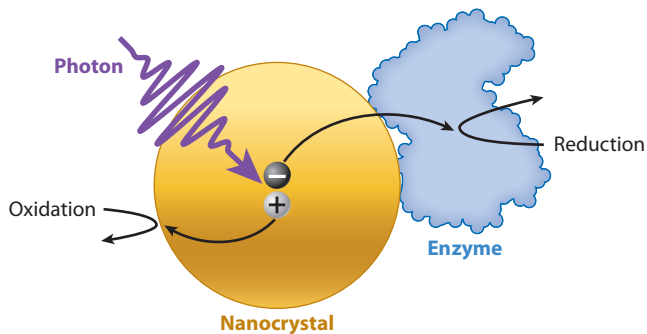


Figure 1

Light-driven reduction chemistry of an NC–enzyme hybrid structure. Light absorption by the NC is followed by transfer of an electron to the enzyme and scavenging of the hole. The electrons transferred to the enzyme participate in reduction catalysis. Abbreviation: NC, nanocrystal.

This review describes the current understanding of the kinetics of ET from an NC to a redox enzyme. This is the key first step in light-driven reduction reactions performed by these systems. The efficiency of ET determines the upper limit on the photochemical activity of the system—if the enzyme were to use all the electrons transferred and the hole scavenging were not rate limiting, the overall photon conversion efficiency would be equal to the efficiency of ET (20, 22, 30, 32). The ET efficiency, in turn, depends on the competition between ET and other electron relaxation pathways. An understanding of the parameters that govern ET can therefore lead to better control of the rate and efficiency of catalysis. In many reports, ET is inferred through detection of photochemical products or photoelectrochemical measurements (11–19, 23, 25–27, 29–31, 33–44, 52). Here, we focus on cases in which NC-to-enzyme ET was studied directly with time-resolved spectroscopy (5, 20–22, 24, 28, 30, 32). Systems combining CdS, CdSe, CdTe, or related heterostructure NCs with enzymes of the hydrogenase (H_2ase) family have served as the prototypical architecture for studying this ET. The synthetic manipulation and tunability of Cd-chalcogenide NCs is well established, and H_2ase structure and function have been extensively characterized (54, 56–58, 62, 63). Both direct NC–enzyme complexation (14, 16, 17, 20–22, 30, 32, 64) and redox-mediated ET (5, 28, 31) have been described, efficient light-driven H_2 production has been demonstrated (14, 16, 17, 21, 28, 30, 31), the kinetics of ET on ultrafast timescales have been characterized (5, 20, 22, 28, 30, 32), and the factors that govern the rate of ET have been explored (20, 21, 28, 31). These foundational studies serve as a framework for understanding the kinetics of ET in other NC–enzyme systems, as illustrated in time-resolved studies of light-driven C–C bond formation (24). For discussions that emphasize photochemical reaction schemes or product detection in NC–enzyme and other biohybrid systems, we refer the reader to other excellent reviews (3, 4, 47, 65–67).

This review is organized as follows: In Section 2, we describe the strategies that have been used to assemble NCs with H_2ases and other enzymes for direct NC-to-enzyme ET. In Section 3, we detail the experiments and kinetic modeling used to probe the kinetics of direct ET. Section 4 focuses on NC– H_2ase systems that use redox mediators to facilitate electron delivery from the NC to the enzyme. In Section 5, we discuss the factors that have been shown to govern the rate of ET in NC– H_2ase systems. In Section 6, we briefly outline the fate of electrons after they have arrived in H_2ases and the factors that govern catalytic activity. In Section 7, we highlight a recent study of NC-to-enzyme ET that leads to C–C bond formation via CO_2 reduction. Finally, in Section 8, we summarize the state of this area of research and lay out some key questions about ET in NC–enzyme systems that remain to be answered.

H_2ase : hydrogenase

2. ASSEMBLY OF NANOCRYSTAL–ENZYME COMPLEXES FOR DIRECT ELECTRON TRANSFER

The ability to tune the ligands on the surfaces of NCs has enabled electrostatic binding to redox enzymes to drive numerous redox reactions through direct charge transfer. Hybrid structures consisting of Cd-chalcogenide NCs with enzymes that are thought to be adsorbed on their surfaces have been used for light-driven H₂ production (14, 16, 17, 21, 30), N₂ fixation (25), NADP⁺ to NADPH conversion (26), C–C bond formation via CO₂ reduction (24), CO₂ reduction to CO (19), sulfite oxidation (27), superoxide oxidation (13), and dehalogenation (43).

In this section, we describe the current understanding of how enzymes bind to NCs. This understanding comes primarily from studies of CdS, CdSe, or CdTe NCs coupled to [FeFe] H₂ase I from *Clostridium acetobutylicum* (*CaI*) and [NiFe] H₂ase from *Thiocapsa roseopersicina* (*Tr*) for light-driven H₂ production (14, 16, 17, 64). By analogy, these principles are thought to apply to other NC–enzyme systems (13, 19, 21, 24, 26, 27, 30, 34, 38–40, 42–44).

2.1. Binding Interactions Between Nanocrystals and Redox Enzymes

In nature, redox equivalents are commonly supplied to redox enzymes by cofactor proteins (4). ET is often enabled through transient protein–protein complexation, promoted by electrostatic interactions between charged amino acid residues (3). For example, ferredoxins—iron–sulfur proteins that act as electron mediators for many redox enzymes—have predominantly negatively charged surfaces that enable binding with positively charged residues on the surfaces of their partner redox enzymes (68, 69). In the case of the [FeFe] H₂ase *CaI*, this type of interaction is thought to lead to selective binding of ferredoxin near the distal [4Fe–4S] cluster of H₂ase, which lies a few angstroms from the surface of the protein and accepts the electron from ferredoxin (3, 70, 71) (Figure 2a). Analogous interactions occur between many other redox enzymes and their native redox partners to facilitate ET (3, 17, 63).

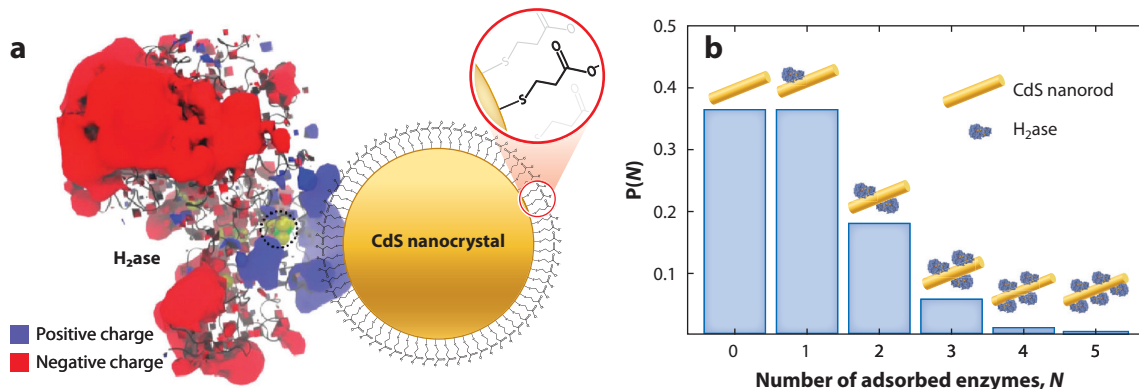


Figure 2

Assembly of NC–H₂ase complexes. (a) Electrostatic surface of [FeFe] H₂ase I from *Clostridium pasteurianum* (a structural homolog of *CaI*), with regions of positive and negative charge shown in blue and red, respectively. A CdS NC capped with negatively charged 3-mercaptopropionate ligands is shown in the location where ferredoxin binds in nature. The relative sizes of H₂ase, NC, and the ligands are drawn approximately to scale for an NC with a 4-nm diameter. (b) Poisson distribution in the number of enzymes bound per CdS NR for $\langle N \rangle = 1$, where N is the number of enzymes adsorbed on an NR. The relative sizes of enzyme and NR are drawn approximately to scale for a 4 × 30-nm NR. Panel a modified with permission from Reference 14; copyright 2010 American Chemical Society. Abbreviations: *CaI*, [FeFe] H₂ase I from *Clostridium acetobutylicum*; H₂ase, hydrogenase; NC, nanocrystal; NR, nanorod.

The assembly of NC–H₂ase complexes is thought to proceed via a biomimetic interaction in which the NC mimics the binding of the native redox partner. The surfaces of colloidal semiconductor NCs are capped by surface-passivating ligands, which enable solubility in an aqueous environment compatible with enzymes, passivate surface defects (58), and—crucially—mediate the interaction between the NC and the enzyme (14, 72). The NC surface chemistry can be tuned to resemble the electrostatic surface of the native redox partner so that the NC binds at the natural electron injection site on the enzyme. Brown and coworkers (14, 16, 17, 20, 21, 30, 64) have used this approach to assemble complexes of CdS, CdSe, or CdTe NCs and [FeFe] H₂ase *Cal* using NCs that have similar dimensions to the native ferredoxin and are capped with negatively charged mercaptocarboxylate ligands (**Figure 2a**). The evidence for this biomimetic binding comes from inhibition of ferredoxin binding to H₂ase in the presence of CdS NRs (16) as well as direct observation of the photoreduction of the distal [4Fe-4S] cluster in CdSe–H₂ase complexes using electron paramagnetic resonance (EPR) spectroscopy (64). Similarly, binding between negatively charged CdTe QDs and a [NiFe] H₂ase *Tr* was hypothesized to occur at the positively charged site of the enzyme surface near the distal or medial iron–sulfur clusters (17). The binding between mercaptocarboxylate-capped Cd-chalcogenide NCs and both [FeFe] and [NiFe] H₂ases has been modeled as a first-order Langmuir isotherm (14, 16, 17, 21). In these systems, the free energy of adsorption is approximately $-10 \text{ kcal mol}^{-1}$ and the adsorption equilibrium constant is approximately 10^6 M^{-1} (14, 16, 17, 21), showing that binding falls in the energy regime that is consistent with physisorption controlled by electrostatic interactions.

Similar electrostatic binding strategies have been implemented in several NC–enzyme systems to drive various redox reactions through direct charge transfer. Most systems studied to date have employed ligands with negatively charged end groups (13, 14, 16, 17, 20–22, 24–26, 30, 32, 34), but positively charged ligands have also been used (12, 13, 34). Because the electrostatic interactions are not sufficiently chemically specific, the orientation in which the enzyme binds to the NC may vary (14, 16, 20, 43), potentially positioning the electron injection site too far from the NC for ET to occur directly. Other binding strategies are being explored as well. For example, [NiFe] H₂ases have been immobilized through covalent linking, whereby the enzyme moiety binds to the surface of the CdS NC either through a histidine tag or peptidic coupling (28, 72). In each of these cases, electrons were shuttled from the NC to the enzyme via redox mediators, rather than injected directly, as discussed in Section 4. Recent developments have used genetic modifications to covalently bind silver nanoclusters to a [NiFe] H₂ase near the distal [4Fe-4S] cluster, thereby hard-wiring the system for direct ET (73). Such approaches may provide inspiration for future NC–enzyme assembly strategies.

2.2. Stochastic Electrostatic Binding Leads to Heterogeneous Populations of Nanocrystal–Enzyme Complexes

Self-assembly of NCs and enzymes in solution driven by electrostatic interactions occurs by stochastic binding events, resulting in a distribution in the number of enzyme moieties bound per NC. For systems in which the NC and enzyme have dimensions on the same order of magnitude and only a few enzymes can bind per NC, these fluctuations are large compared to the mean number of enzyme moieties bound per NC, $\langle N \rangle$. It is therefore important to account for this population heterogeneity to accurately describe ET rates and binding in NC–enzyme complexes (22, 32). This is in contrast to cases where many charge acceptors can interact with a single NC (e.g., small-molecule acceptors) such that averages are sufficient to describe the distribution (74).

When NCs and enzymes are mixed at low molar ratios such that $\langle N \rangle$ is small compared to the maximum number of available binding sites on each NC, the number of adsorbed enzymes

Transient absorption

(TA): a pump-probe spectroscopy technique that measures the evolution of photoexcited states in time

per NC (N) follows the Poisson distribution $P(N) = \langle N \rangle^N e^{-\langle N \rangle} / N!$ (16, 22, 30, 32, 75–79). The Poisson distribution in the number of enzyme moieties bound per NR for $\langle N \rangle = 1$ is depicted in **Figure 2b**. The value of $\langle N \rangle$ in an ensemble solution is governed by the binding equilibrium thermodynamics, the molar mixing ratio of the enzyme and NCs, and the absolute concentrations of both species in solution. While the Poisson distribution is appropriate when $\langle N \rangle$ is much smaller than the maximum capacity of the NC surface, as in the case of CdS NRs (16, 22, 30, 32), high enzyme loading that approaches saturation of the NC would be better described by the binomial distribution (32, 76, 80). This is likely to be the case in systems that use smaller NCs such as QDs, which are comparable in size to the enzymes and have a limited surface area for enzyme adsorption (21). Geometric models for the dense packing of enzyme moieties on the NC surface have also been developed to describe enzyme binding near saturation of surfaces of CdTe QDs (i.e., when $\langle N \rangle$ approaches the number of available binding sites) (21). As we describe in the next section, a description of the population heterogeneity in ensembles of NC–enzyme complexes is essential for a quantitative understanding of ET kinetics and efficiencies.

3. ELECTRON-TRANSFER KINETICS IN NANOCRYSTAL–HYDROGENASE COMPLEXES

In this section, we review the time-resolved spectroscopy methods that have been employed to examine the kinetics of direct ET from CdS NRs and CdTe QDs to [FeFe] H₂ase *Cal* adsorbed on the NC surface (20–22, 30, 32). Because excited-state decays of NCs are often complex and multiexponential, extraction of rate constants for ET requires kinetic modeling of the time-resolved data. This section describes the results of transient absorption (TA) spectroscopy and time-resolved photoluminescence (TRPL) experiments and the kinetic modeling used to characterize the ET process.

3.1. Rates and Efficiencies of Electron Transfer from CdS Nanorods to Hydrogenase

TA spectroscopy provides a way to probe charge-transfer dynamics over a broad range of timescales relevant to interfacial charge transfer and intrinsic NC relaxation (20, 22, 30, 32, 55, 81–87). TA spectra of semiconductor NCs have features that report on the populations of photoexcited electrons and holes in various excited states from which charge transfer occurs (85, 87–89). In Cd-chalcogenide NCs in particular, the magnitude of the band-edge bleach signal in the visible region is directly proportional to the population of electrons in the conduction band, with only minor contributions from holes in the valence band (84, 88, 90, 91). Therefore, monitoring this signal allows for the direct observation of electron population dynamics, including ET. In the presence of an electron acceptor, ET causes the photoexcited electron population to decay more quickly than in free NCs (**Figure 3a**), and a comparison of the electron decay kinetics in these two cases can be used to extract ET kinetics.

TA spectroscopy, in conjunction with kinetic modeling, has been employed to measure the rate constants and efficiencies of ET in complexes of CdS NRs and [FeFe] H₂ase (20, 22, 28, 30, 32). In the absence of H₂ase, photoexcited charge carriers in CdS NRs can undergo a variety of relaxation pathways, including trapping and electron–hole recombination (77, 92–94), as depicted in **Figure 3b**. Ensemble samples of photoexcited NCs typically exhibit multiexponential decay kinetics over a broad range of timescales due to population heterogeneity and multiple relaxation pathways (77, 92–94) (see the sidebar titled Nanocrystal Excited-State Dynamics). Moreover, the distribution in the number of bound enzyme moieties described in Section 2.2 produces an additional layer of complexity in the ET kinetics (22, 32).

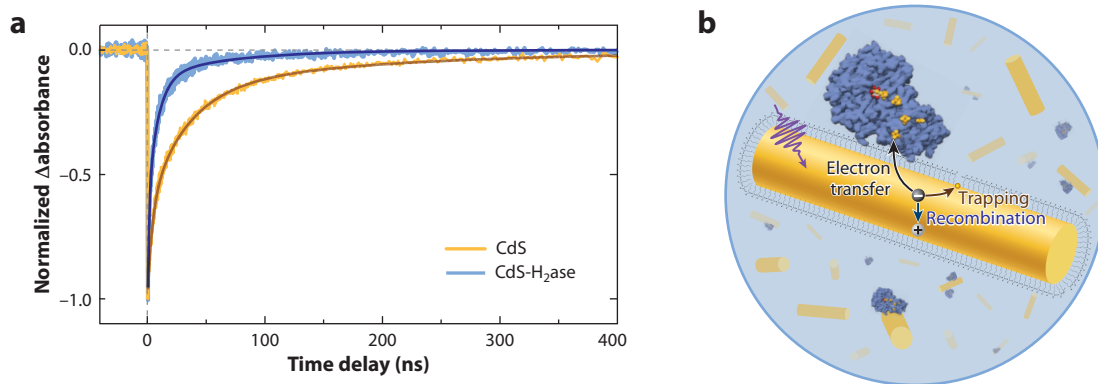


Figure 3

Measuring ET kinetics in CdS–H₂ase complexes using TA spectroscopy. (a) The decay of the band-edge bleach signal of CdS NRs with and without [FeFe] H₂ase *Cal*. In the presence of the enzyme, the electron lifetime is shortened due to ET from the NC to the enzyme. (b) ET from a CdS NR (yellow cylinder) to an [FeFe] H₂ase (blue protein surface rendering) adsorbed on the surface after absorption of a photon (purple arrow) by the NR and the competing relaxation pathways of the NC, such as electron trapping and recombination. Panel a modified with permission from Reference 20; copyright 2014 American Chemical Society. Panel b modified from Reference 22 with permission from the PCCP Owner Societies. Abbreviations: *Cal*, [FeFe] H₂ase I from *Clostridium acetobutylicum*; ET, electron transfer; H₂ase, hydrogenase; NC, nanocrystal; NR, nanorod; TA, transient absorption.

ET from an NC to each bound enzyme occurs with a rate constant k_{ET} , an intensive quantity that allows for quantitative comparisons across different systems (55). The competition between ET and the other relaxation processes in the NC determines the quantum efficiency of ET (ϕ_{ET}), which in turn determines the upper limit of the photochemical activity (22). In early time-resolved studies of ET in CdS NR–H₂ase complexes, the rate constant of ET was estimated using average lifetime analysis (95). This analysis showed that ET and competing electron relaxation pathways occurred on similar timescales and thus were in direct kinetic competition. Kinetic modeling that accounts for nonexponential NC decay and enzyme number distributions in CdS NR–[FeFe] H₂ase complexes was subsequently developed to obtain k_{ET} quantitatively (22, 30, 32) following the precedent of heterogeneous charge-transfer kinetics in micellar and other NC–acceptor

NANOCRYSTAL EXCITED-STATE DYNAMICS

We briefly describe the intrinsic excited-state dynamics of NCs that are relevant to determining the efficiency of ET in NC–enzyme systems. The absorption of a photon by a semiconductor NC generates an excited electron–hole pair. These photoexcited charge carriers can go through several radiative and nonradiative relaxation pathways over a broad range of timescales (77, 92–94). In CdS nanorods, in particular, the primary decay pathways that compete with ET are electron trapping to localized surface sites and electron–hole recombination, as depicted in **Figure 3b**. These processes occur on timescales of nanoseconds and tens of nanoseconds, respectively (20, 22, 30, 32). In an ensemble sample of colloidal semiconductor NCs, structural and environmental heterogeneities give rise to distributions in the rates of the various decay pathways, leading to multiexponential decay kinetics over picosecond to microsecond timescales (77, 92–94). For example, the band-edge bleach of CdS nanorods exhibits multiexponential decay originating from a distribution in the number of electron traps per NC (22). These details are important for kinetic modeling of ET in NC–enzyme complexes, as described in the main text.

systems (75–79). For the Poisson distribution in the number of enzyme moieties bound per NC described in Section 2.2, the electron survival probability is given by (22, 75–79)

$$S_{\text{DA}}(t) = S_{\text{D}}(t) \exp[\langle N \rangle (e^{-k_{\text{ET}}t} - 1)], \quad 1.$$

where $S_{\text{D}}(t)$ and $S_{\text{DA}}(t)$ are the survival probabilities of the excited electron in the NC (donor, D) in the absence and presence of enzymes (acceptors, A), respectively. The ET efficiency for a system that exhibits nonexponential NC relaxation kinetics, as well as a distribution in the number of enzyme moieties bound, can be calculated using empirical decay functions for the NC in the absence [$S_{\text{D}}(t)$] and presence [$S_{\text{DA}}(t)$] of enzymes using the following expression (32):

$$\phi_{\text{ET}} = 1 - \int_0^{\infty} dt k_{\text{D}}(t) S_{\text{DA}}(t), \quad 2.$$

where $k_{\text{D}}(t) = -\frac{dS_{\text{D}}(t)/dt}{S_{\text{D}}(t)}$ represents the time-dependent rate constant of the donor decay (96).

The experimental methods and analysis described above showed that when CdS NRs are capped with 3-mercaptopropionate ligands, ET to bound H₂ase occurs on the timescale of tens of nanoseconds: $k_{\text{ET}} 10^7$ – 10^8 s⁻¹ (22, 30, 32). Kinetic modeling also provided the rate constants for recombination and electron trapping in the CdS NRs (**Figure 3b**; also see the sidebar titled Nanocrystal Excited-State Dynamics), which were on the orders of 10^7 s⁻¹ and 10^8 s⁻¹, respectively. The number of electron traps per NR was small, with an average below 1, making electron trapping play a minor role in this particular system. ϕ_{ET} was 30–40% when CdS and H₂ase were mixed in a 1:1 ratio (32). These studies showed that a 100-fold increase of k_{ET} compared to the NC recombination rate constant could yield significant gains in the efficiency of ET and therefore the photochemical activity of this model NC–enzyme system. Such improvements could be made by synthetic means, as discussed below in Section 5.

3.2. Electron Transfer from CdTe Quantum Dots to Hydrogenase

TRPL is another common method for studying charge-transfer dynamics in NC–acceptor complexes (21, 77, 92). The band-gap photoluminescence emission peak in the spectra of NCs reports on the population of electrons and holes, and its decay is determined by the shorter-lived carrier. Shortening of the photoluminescence lifetime in the presence of electron acceptors can report on ET kinetics, provided that the quenching can be attributed to the carrier in question (21, 77, 92). TRPL was used to characterize the kinetics of ET from CdTe QDs with a range of diameters capped with 3-mercaptopropionate ligands to [FeFe] H₂ase *Cal* (21). The CdTe QDs used in the study have a smaller surface area than the CdS NRs described above and thus can accommodate only a small number of enzyme moieties, requiring a different description of binding than that discussed in Section 2.2. To measure the average rate constant of ET, the authors compared the average lifetimes of free QDs and QDs for which the surface was saturated with H₂ase moieties. The average single-acceptor ET rate constant was then estimated by dividing by the maximum number of H₂ase bound at saturation. The maximum number of H₂ase moieties able to bind to a QD was estimated by developing two geometric binding models that treated the enzyme footprint as either conical or elliptical in shape. This approach gave average k_{ET} values between 5 and 9×10^6 s⁻¹, depending on the NC size and binding model used. The interpretation of the dependence of k_{ET} on the QD diameter is described in Section 5.2. The factors that may determine the value of k_{ET} are the subject of Section 5.

k_{ET} : rate constant of electron transfer

Internal quantum efficiency of electron transfer (ϕ_{ET}): the probability that an excited electron undergoes electron transfer to the acceptor rather than relaxation within the donor

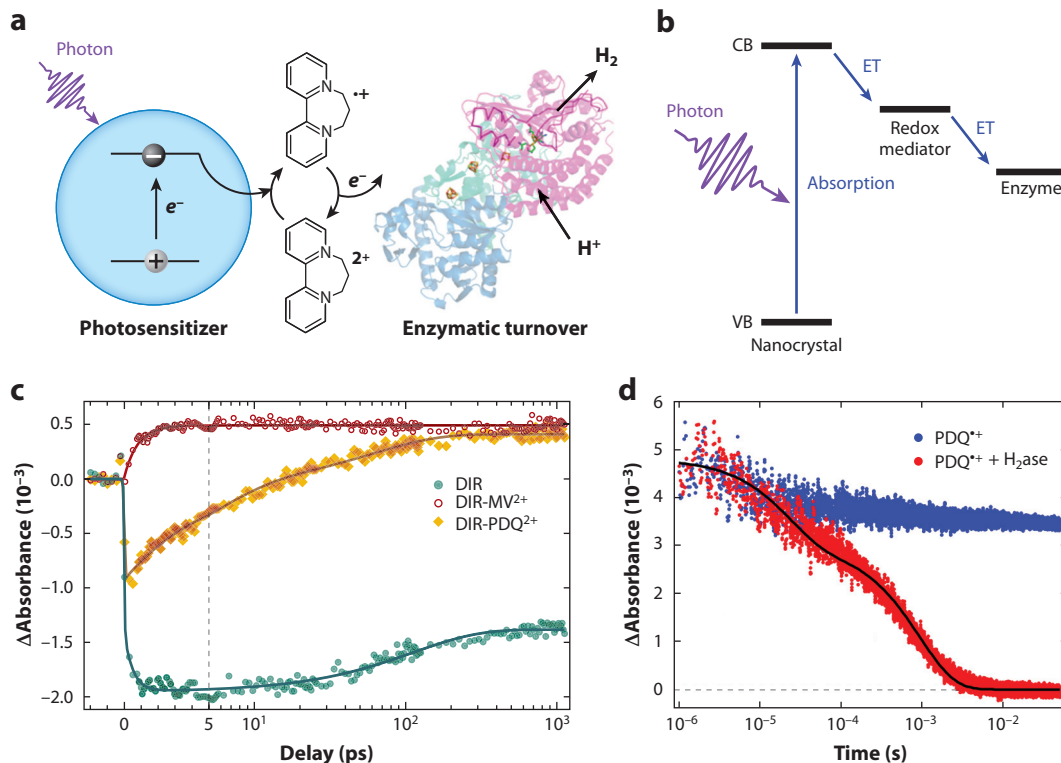


Figure 4

NC-to-enzyme ET via redox mediators. (a) Redox-mediated ET and enzymatic turnover using an NC-PDQ²⁺-[NiFe] H₂ase system. (b) Generic energy-level diagram for ET in NC-redox mediator-enzyme systems depicting the two-step ET between the NC and the enzyme after excitation of an electron in the NC from the VB to the CB. (c) TA time traces at a probe wavelength of 490 ± 5 nm for photoexcited CdSe/CdS DIR heterostructures (green filled circles), DIR-MV²⁺ (red open circles), and DIR-PDQ²⁺ (yellow diamonds). At this probe wavelength, there is a negative bleach proportional to the population of electrons in the NC and a PA feature that appears when the charge-separated state is formed after ET. The increasingly positive amplitudes signify ET. The time axis is linear for the first 5 ps (gray dashed line) and logarithmic thereafter. (d) Time-resolved signal at 808 nm showing ET from PDQ⁺ to [NiFe] H₂ase after initial photoexcitation of CdSe/CdS DIR heterostructures. Panels a and d adapted with permission from Reference 5; copyright 2017 American Chemical Society. Panel b modified from Reference 31; copyright 2019 Chemical Communications. Panel c adapted from Reference 28 with permission of the Royal Society of Chemistry. Abbreviations: CB, conduction band; DIR, dot-in-rod; ET, electron transfer; H₂ase, hydrogenase; MV²⁺, methyl viologen; NC, nanocrystal; PA, photoinduced absorption; PDQ²⁺, propyl-bridged 2-2'-bipyridinium; TA, transient absorption; VB, valence band.

4. REDOX-MEDIATED ELECTRON TRANSFER FROM NANOCRYSTALS TO ENZYMES

In addition to hybrid structures where enzymes are directly adsorbed on particle surfaces, architectures in which the ET between an NC and an enzyme is mediated by a redox shuttle have been developed. Within this architecture, a photon is absorbed by the NC, the photoexcited charge transfers to the redox mediator, which shuttles the charge to or from the enzyme (Figure 4a,b). This system differs from NC-enzyme complexes described in Sections 2 and 3 in that ET—and, ultimately, catalysis—relies on transport of the charge carrier via the redox mediator. Examples of reactions achieved in this manner include proton-to-H₂ conversion (16, 30, 31),

stereospecific reduction chemistry (18), photoelectrochemical sensing of sugars via oxidation of fructose and glucose (15, 29), the reduction of various aldehydes to alcohols (26), monooxygenation of myristic acid (11), nitrate reduction (12), oxidation of lactate (12), and phosphorylation of guanosine monophosphate to guanosine diphosphate (23). Most systems investigated thus far have used solvated redox-active molecules to shuttle electrons between the NC and enzyme in solution (5, 15, 16, 18, 28–31, 52). In other cases, enzymes themselves or enzyme-catalyzed products act as the mediator, shuttling electrons between the NC and other enzymes (12, 23, 26), or alternatively the NCs and enzyme can be entrapped in a redox-active polymer matrix (29). Here, we focus on systems utilizing CdSe QDs or CdSe/CdS dot-in-rod (DIR) heterostructures and H₂ase, in which the kinetics of ET and the factors that control ET rates have been directly investigated (5, 28, 31).

The overall efficiency of charge transfer in NC–mediator–enzyme systems depends on the efficiencies of the individual sequential steps of charge transfer between the NC and the mediator, transport of the charge via the redox mediator, and charge transfer between the mediator and the enzyme (**Figure 4a,b**). To map out the ET pathways and their timescales in NC–mediator–H₂ase systems, Greene, Chica, and coworkers (5, 28) performed a series of time-resolved visible and IR spectroscopy experiments on solutions of CdSe/CdS DIR NCs and [NiFe] H₂ase from *Pyrococcus furiosus* (*Pf*), with methyl viologen (MV²⁺) and propyl-bridged 2–2'-bipyridinium (PDQ²⁺) acting as redox mediators. In their studies, the enzyme was suspected to bind to the NC via a polyhistidine tag on the H₂ase surface (11, 28, 97). While this molecular linker does not allow for direct ET—as it creates a distance too great for direct electron injection—it shortens the distance that the redox mediator must travel. To monitor the ET kinetics of this system, TA spectroscopy was used to investigate the first ET event (from the DIR to the mediator) using a probe spectral region (490 ± 5 nm) that exhibits a negative bleach signal when the photoexcited electron is in the NC and becomes a positive photoinduced absorption feature when the charge-separated state is formed after ET (**Figure 4c**). The negative signal of DIRs in the absence of redox mediators decayed only partially over the nanosecond time window due to intrinsic relaxation of the NC. The increasingly positive signal observed in the presence of the redox mediators shows that ET occurs on a subpicosecond timescale for both redox mediators, making its efficiency near unity (27) (**Figure 4c**). They separately monitored the TA signal associated with the redox mediators in the presence and absence of the H₂ase (5). The second ET event (from the reduced, radical form of the redox mediator to H₂ase) was found to occur on the microsecond to millisecond timescale for PDQ^{•+} (**Figure 4d**) and after milliseconds for MV^{•+}. PDQ²⁺ was a superior redox mediator to MV²⁺, as its reduced form was fully consumed over the duration of the experiment, while MV^{•+} maintained considerable signal over the same time window. A high internal quantum efficiency of H₂ production of about 77% was achieved when using PDQ²⁺, indicating a high overall NC-to-enzyme ET efficiency. As discussed in Section 5.2, the use of MV²⁺ as a redox mediator did not lead to significant H₂ production.

Architectures that rely on redox mediators to shuttle electrons between NCs and enzymes have several advantages and disadvantages compared to direct ET in bound NC–enzyme complexes. Redox-mediated systems are not subject to the challenges of achieving the biomimetic binding orientations required for direct ET. In addition, molecular acceptors capable of permeating the NC ligand layer can facilitate ET that is faster and therefore more efficient than direct charge transfer to enzymes, which have redox active accessory clusters buried inside the enzymes (28, 98) (**Figure 2**). While indirect transfer via the mediator makes the overall rate of ET slow compared to direct ET, the efficiency can be substantial if the reduced or oxidized mediator is stable on the timescale of its transport to the enzyme, because the first ET event outcompetes other relaxation pathways in the NC (16, 28, 31). Along with efficient charge transfer, the possibility

of back-charge transfer to the NC is reduced when compared to a directly complexed system because the interaction between the NC and mediator is transient. However, in a solution-phase redox-mediated system, the upper limit on the rate of product formation is defined by transport of the redox mediator or by the rate of enzyme catalysis, similar to redox enzymes *in vivo*. Additionally, instability of the excited redox molecule (e.g., due to radical intermediates) and undesired side reactions are potential challenges of this system design (8). It remains to be seen whether redox mediators are suitable for reactions involving several sequential intermediate steps, such as the eight-electron reaction for conversion of N₂ into ammonia (99).

5. FACTORS THAT DETERMINE k_{ET} IN NANOCRYSTAL-HYDROGENASE SYSTEMS

The rate of interfacial ET in many NC-acceptor systems has been described within the framework of Marcus theory for classical, nonadiabatic ET (100):

$$k_{\text{ET}} = \frac{2\pi}{\hbar} |H_{\text{DA}}|^2 \frac{1}{\sqrt{4\pi\lambda k_{\text{B}}T}} \exp\left[-\frac{(\Delta G + \lambda)^2}{4\lambda k_{\text{B}}T}\right]. \quad 3.$$

Here, $|H_{\text{DA}}|^2$ is the electronic coupling between the donor and acceptor, ΔG is the free energy difference between the initial and final states ($-\Delta G$ is commonly referred to as the driving force), λ is the reorganization energy that corresponds to the energy cost of putting the donor-acceptor pair in the nuclear geometry of the charge-separated state, k_{B} is the Boltzmann constant, and T is the temperature. Marcus theory, which has successfully described interfacial charge transfer between NCs and both molecular and various solid-state acceptors, provides a starting point for controlling k_{ET} by rational design (55). Below, we review what is known about the impact of the parameters that appear in Equation 3 on ET from NCs to H₂ases.

5.1. Electronic Coupling Between Nanocrystals and Hydrogenase

According to Marcus theory, k_{ET} is directly proportional to the electronic coupling between the donor and acceptor, $|H_{\text{DA}}|^2$ (Equation 3). In many cases, the interface between the NC donor and the acceptor is defined by the surface-capping ligands of the NC (3, 30, 55, 87). These ligands can act as a tunneling barrier such that the electronic coupling, and in turn k_{ET} , falls off exponentially with the donor-acceptor distance:

$$k_{\text{ET}}(d) = k_{\text{ET}}(0)e^{-\beta d}, \quad 4.$$

where d is the donor-acceptor distance, β is the attenuation factor, and $k_{\text{ET}}(0)$ is the ET rate constant in the hypothetical case where there is no separation between the donor and acceptor (101). An effective way to control the electronic coupling is through controlling the chemical structure, which strongly impacts β , or the length of the bridge that separates the donor and acceptor, which affects d . This approach has been successfully employed to control k_{ET} in NC-acceptor systems by using conducting ligands and shorter ligands (102–106).

Surface-capping ligands have been shown to impact the value of k_{ET} in electrostatically bound complexes of CdS NRs and [FeFe] H₂ase *Cal* (30) (Figure 5). Using a series of mercaptocarboxylate ligands of varying lengths (Figure 5a), Wilker et al. (30) showed that k_{ET} increases exponentially with decreasing ligand length (Figure 5b). In an analogous experiment performed on H₂ase electrostatically immobilized onto an Au electrode functionalized with mercaptocarboxylate self-assembled monolayers, the TOF was found to increase exponentially

$|H_{\text{DA}}|^2$: electronic coupling between donor and acceptor

ΔG : free energy difference between the initial and final states of the ET process

λ : reorganization energy

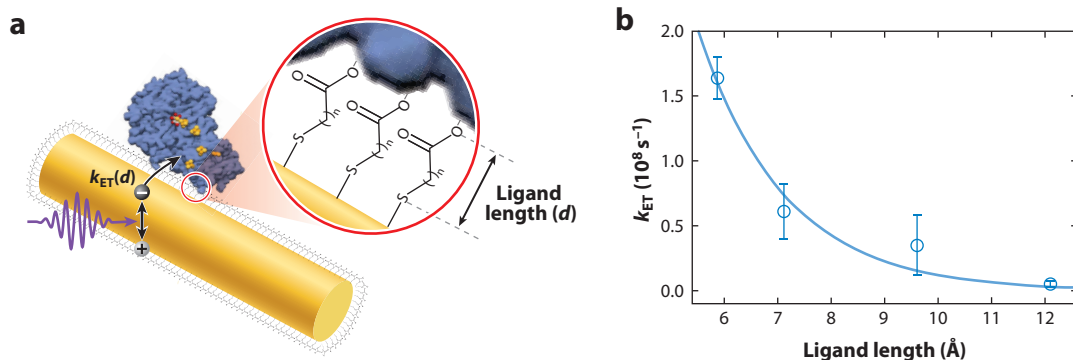


Figure 5

Controlling k_{ET} , the rate constant of ET, through electronic coupling in NC–H₂ase complexes. (a) ET from a CdS NR to [FeFe] H₂ase, which is controlled by the length of the ligand layer, d . The relative sizes of H₂ase, the NR, and the ligands are drawn approximately to scale for an NR with a 4-nm diameter. (b) Experimentally measured exponential dependence of k_{ET} on ligand length in complexes of CdS NRs and [FeFe] H₂ase *Cal*. Figure adapted with permission from Reference 30; copyright 2018 American Chemical Society. Abbreviations: *Cal*, [FeFe] H₂ase I from *Clostridium acetobutylicum*; ET, electron transfer; H₂ase, hydrogenase; NC, nanocrystal; NR, nanorod.

with decreasing length of the mercaptocarboxylate (107). In both cases, the value of β measured is consistent with the electron tunneling through the saturated alkane chains ($0.7\text{--}1.3 \text{ \AA}^{-1}$) (30, 101, 103, 105, 107). These studies suggested that k_{ET} could be improved drastically if the ligand barrier were very short or removed altogether.

5.2. Driving Force for Electron Transfer

Brown et al. (21) investigated the role of driving force on direct ET in bound complexes of CdTe QDs and [FeFe] H₂ase *Cal* by measuring the average k_{ET} as a function of QD diameter. There, ΔG was defined as the difference between the free energy of the conduction-band minimum of the QD and the distal iron–sulfur cluster of H₂ase. Due to quantum confinement, ΔG increases with decreasing particle size. They found that k_{ET} did not depend on ΔG for this system and postulated that ET to H₂ase is gated (i.e., coupled to a chemical step), such as proton-coupled ET. While changes to the NC diameter affect ΔG , the curvature of the surface also changes dramatically with diameter, potentially affecting the geometry at the binding pocket and the effective donor–acceptor distance. They may affect the value of $|H_{DA}|^2$. More work is needed to disentangle the correlated effects of particle size, driving force, and binding interactions in this system.

In contrast, the driving force for ET has been found to play a key role in systems that utilize redox mediators. Chica et al. (28) investigated two different mediators, MV²⁺ and PDQ²⁺, in a system consisting of CdSe/CdS DIR NCs and [NiFe] H₂ase *Pf* tethered using a histidine tag. The midpoint potential of PDQ²⁺ is about 100 mV more negative than that of MV²⁺, resulting in different driving forces for ET for the two mediators. While ET from the NC to both MV²⁺ and PDQ²⁺ is fast, only PDQ²⁺ was able to drive enzymatic H₂ production. The authors concluded that the added driving force for ET from the mediator to H₂ase was a key factor for product formation. TA spectroscopy measurements showed that ET from the NCs to MV²⁺ was faster than to PDQ²⁺ (28) (**Figure 4c**), which was attributed to the higher driving force for ET to MV²⁺. However, both processes were fast enough to have essentially unity efficiency. ET from PDQ²⁺ to H₂ase, measured by time-resolved IR spectroscopy, was much faster and more efficient than

from MV^{2+} (**Figure 4d**), enabling overall charge transfer from photoexcited CdSe/CdS to H_2ase (5). In a follow-up study, a series of five redox mediators was used to investigate how the midpoint potential of the mediator influences the efficiency of ET from CdSe QDs to the mediator, as well as the resulting light-driven H_2 production by CdSe QDs and [NiFe] H_2ase *Pf* (31). ET from the NC to the mediator became monotonically more efficient as the mediator midpoint potential became more positive, while H_2 production exhibited a peak in its efficiency at an intermediate mediator midpoint potential. This was interpreted as the reciprocal effect of driving force on these two ET processes, where more positive mediator midpoint potentials give a larger driving force for ET from the NC to the mediator but a smaller driving force from the mediator to the enzyme (**Figure 4b**). The desired configuration is one in which the total energy difference is split between the first and second ET step to optimize the total ET efficiency. Using the optimized mediators for the CdSe QD and CdSe/CdS DIR systems, high internal quantum efficiencies of H_2 production of about 17% (31) and 77% (28), respectively, were achieved. The enhanced efficiencies with the DIR heterostructures were attributed to longer excited-state lifetimes and slower back-ET (28).

These results described above highlight the intrinsic differences between direct and redox-mediated ET. Systems that utilize direct complexation are sensitive to small system variations that affect binding orientation and the distance between the NC surface and the electron injection site because changes in NC diameter could affect both ΔG and $|H_{DA}|^2$. Redox-mediated systems where the mediators can move close to the electron donor and acceptor sites are sensitive to balancing of driving forces of two ET steps. The precise mechanism of ET and involvement of other reactants such as protons may vary with the location of the ET event. To complicate matters further, surface-capping ligands can shift the energy levels of NCs and impact the value of ΔG for ET from them (108, 109). Furthermore, recent studies on ET from Cd-chalcogenide NCs to molecular acceptors suggest that the so-called Marcus-inverted regime, where k_{ET} falls off with increasing driving force because $-\Delta G > \lambda$ (Equation 3), is not observed when strong electron-hole interactions in quantum-confined NCs enable Auger-assisted ET (87, 110, 111). This behavior may also be at play in NC-enzyme complexes.

5.3. Reorganization Energy

The role of reorganization energy in determining k_{ET} in NC-enzyme complexes has not been explored systematically. However, it has been postulated that the enzyme contribution dominates λ (21). For charge transfer in NC-molecular acceptor systems, the NC has been found to constitute a relatively small contribution (1–100 meV) to the total reorganization energy (83, 87, 112, 113). In contrast, reorganization energies for changing the oxidation state of metal centers in redox enzymes that act as the charge injection site are typically approximately 1 eV (114, 115). In redox-mediated systems, λ for ET both to and from the mediator should be considered (31).

6. EVENTS FOLLOWING ELECTRON TRANSFER FROM NANOCRYSTALS TO HYDROGENASES

While ET from an NC to an enzyme is a critical early step in light-driven catalysis and is the focus of this review, it is followed by other steps involved in enzyme catalysis, as well as potential back-ET to the NC. Here, we briefly discuss what is known about the fate of the electron once it is injected from an NC to H_2ase and how the kinetics of the NC-to- H_2ase ET step relate to the overall catalytic cycle.

Midpoint potential: electrochemical potential where the ratio of reduced and oxidized species is equal to one

6.1. Electron Transport Within Hydrogenases

In many redox enzymes, including H₂ases, electrons are injected into a metal center—known as an accessory iron–sulfur cluster—near the surface of the enzyme, while the catalytically active site lies further inside the enzyme (5, 14, 16, 17, 20, 116). Once an electron has transferred from the NC to the enzyme, it must undergo one or more charge-transfer steps along the electron transport chain within the enzyme before it can participate in catalysis at the active site (20) (**Figure 6a**). This intraprotein ET process commonly occurs via accessory iron–sulfur clusters, and the rates of forward and backward electron flow are dictated by the electronic properties of each cluster as well as by the enzyme structure (114, 115), as reviewed in detail elsewhere (115).

Intraprotein electron transport and reaction pathways following electron injection from an NC have been investigated in [NiFe] H₂ase I *Pf*, [NiFe] H₂ase *Tr*, and [FeFe] H₂ase *CaI* (5, 17, 64). The behavior of electrons inside the enzyme cannot be readily observed with visible spectroscopy, as the signals of the redox enzyme in this region of the electromagnetic spectrum are much weaker than those of NCs (20). Fourier-transform infrared (FTIR) and EPR spectroscopies are superior tools for examining enzyme behavior in the presence of NCs (5, 17, 64) (**Figure 6**). FTIR spectroscopy on bound complexes of CdTe QDs and [NiFe] H₂ase *Tr* was used to monitor changes in the vibrational bands associated with the CO and CN⁻ ligands bonded to Fe and Ni at the H₂ase active site after photoexcitation of the NC (17). These signals are sensitive to the oxidation state of the active site. The resting state of the enzyme active site was converted to the reduced, catalytically active form over the course of illumination due to the electron injection from the NCs (**Figure 6b**). Separately, FTIR spectroscopy over a range of temperatures was used to track changes of the oxidation state of the active site of the [FeFe] H₂ase *CaI* upon ET from CdSe QDs on the timescale of seconds, revealing that catalysis proceeds through thermally activated, proton-dependent steps (64). In the same study, the electron pathway was probed with EPR spectroscopy to track the oxidation states of the accessory iron–sulfur clusters that make up the intraprotein electron transport chain (64). Under illumination of the NC, EPR spectra showed evidence of reduction of both the enzyme active site and accessory iron–sulfur clusters (**Figure 6c**), supporting the hypothesis that the electron injection site was the distal [4Fe-4S] cluster near the surface of the enzyme—the same cluster that receives an electron from the native ferredoxin electron donor (**Figure 6a**). More recently, time-resolved IR measurements on the millisecond timescale were reported (**Figure 6d**), narrowing the gap between ultrafast spectroscopic experiments on NC-to-enzyme ET and steady-state product detection by resolving the kinetics of catalysis in an NC–enzyme system (5). These measurements provided new insights about the catalytic mechanism of [NiFe] H₂ase *Pf*.

Together, these studies present direct evidence for photoexcited ET from NCs into [NiFe] and [FeFe] H₂ases, provide information about NC–H₂ase binding, and reveal mechanistic insights into H₂ase catalysis. H₂ases can exhibit fast rates of catalysis (greater than 10³ s⁻¹) (107), rendering their mechanisms challenging to study (5). NC–H₂ase systems have thus opened new avenues for resolving H₂ase reaction mechanisms (5). With continuing interest in mechanisms of redox enzyme catalysis (5, 63, 64), hybrid NC–enzyme systems may be a valuable tool for probing the behavior of enzymes.

6.2. Relationships Between Electron Transfer and Catalysis in Nanocrystal–Hydrogenase Systems

The catalytic activity of NC–enzyme systems is determined by a complex interplay of multiple factors. Examples include excitation rate, ϕ_{ET} , competition for photoexcited charges between enzymes, back-transfer of charges between the NC and the enzyme after the formation of

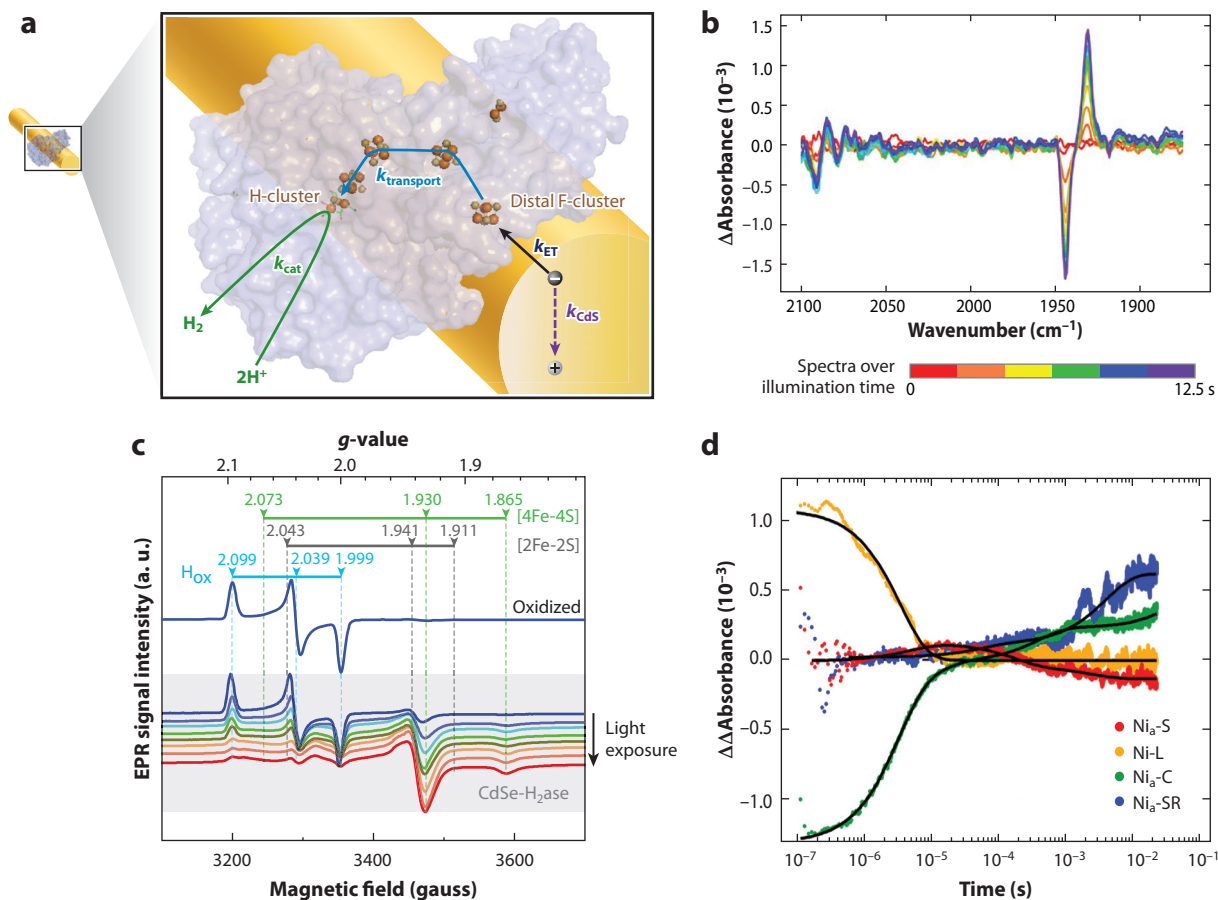


Figure 6

Fate of electrons after injection from a photoexcited NC into H₂ase. (a) The electron pathway in CdS NR–[FeFe] H₂ase complexes that leads to H₂ generation. The enzyme structure shown is that of [FeFe] H₂ase I from *Clostridium pasteurianum*, a structural homolog to *Cal*. The enzyme surface is shown in gray with the iron and sulfur atoms of the iron–sulfur clusters shown as orange and yellow spheres, respectively. The electron injection site is known as the distal F-cluster, and the catalytically active site is known as the H-cluster. The rate constant of intrinsic electron decay in CdS is denoted by k_{CdS} , the rate constant of electron injection from CdS to H₂ase by k_{ET} , the rate constant of electron transport through H₂ase to the H-cluster by $k_{\text{transport}}$, and the rate constant of H₂ production by k_{cat} . (b) Direct evidence of NC-to-enzyme ET in complexes of CdTe QDs and [NiFe] H₂ase *Tr*, probed by FTIR spectroscopy. Difference spectra over illumination time, ranging from 0 s (red) to 12.5 s (purple), show photoinduced reduction of the H₂ase active site, monitored through frequency shifts of the CO and CN[−] ligands of the active site. (c) EPR spectra of CdSe–H₂ase *Cal* complexes collected after illumination for consecutive 10–20 s intervals going from blue to red, showing the H_{ox} signal giving way to a signal assigned to reduced distal iron–sulfur clusters over time. (d) IR transients corresponding to the indicated intermediates of the active site of the [NiFe] H₂ase *Pf*: Ni_a-S is the resting state, Ni-L is the reduced and protonated intermediate, Ni_a-C has a hydride intermediate, and Ni_a-SR contains the hydride and a nearby protonated thiol that precedes H₂ generation. Panel a modified with permission from Reference 20; copyright 2014 American Chemical Society. Panel b modified with permission from Reference 17; copyright 2014 American Chemical Society. Panel c modified with permission from Reference 64; copyright 2014 American Chemical Society. Panel d modified with permission from Reference 5; copyright 2014 American Chemical Society. Abbreviations: *Cal*, [FeFe] H₂ase I from *Clostridium acetobutylicum*; EPR, electron paramagnetic resonance; ET, electron transfer; FTIR, Fourier-transform infrared; H₂ase, hydrogenase; H_{ox}, oxidized active site; IR, infrared; NC, nanocrystal; QD, quantum dot.

TOF: turnover frequency

Photochemistry: chemical reactions activated by light

intermediates, regeneration of NC ground state by a charge donor, availability of reactant substrates, and the fraction of catalytically active enzymes in the sample. Here, we outline the role of some of these factors in governing photochemical H₂ production in NC–H₂ase systems.

In nature, the rate of catalytic turnover by redox enzymes such as H₂ases is limited by the diffusion-controlled protein–protein interactions in solution (2–4, 16). The architecture of bound NC–enzyme complexes is designed to drive catalysis faster than the diffusion limit such that the turnover frequency (TOF), in units of product molecules produced per enzyme per second, is limited by the excitation frequency, efficiency of ET, and intrinsic rate of catalysis, k_{cat} . In the photon-limited regime, the TOF of H₂ production is directly proportional to the excitation frequency, ν_{ex} . Provided that $k_{\text{ET}} \gg \nu_{\text{ex}}$, the rate of electron injection into the enzyme is given by $\nu_{\text{ex}}\phi_{\text{ET}}$, where ϕ_{ET} quantifies the competition between ET and other excited-state decay processes in the NC (see Section 3.1). If there are no losses within the enzyme after ET and k_{cat} is fast, this product will also equal the TOF. Under monochromatic light intensity that approximates the absorption of solar photons, light-driven H₂ production by bound CdS–[FeFe] H₂ase *Cal* complexes was found to be limited by the electron injection rate and not by the inherent catalytic turnover rate (16). Extrapolation of single-molecule measurements of [FeFe] H₂ase (from *Cal*) driven by an Au electrode suggest that a TOF of at least 10⁴ s^{−1} may be possible if electrons could be supplied at a fast-enough rate (107). This could be achieved by exciting the NCs at high excitation rates, provided that the ET is efficient and hole scavenging is fast enough to regenerate the ground state.

Prior work on bound complexes with a 1:1 CdS NR:[FeFe] H₂ase *Cal* molar mixing ratio reported that the values of ϕ_{ET} were similar to the internal quantum efficiency of H₂ production (both about 20%) (16, 22), suggesting that [FeFe] H₂ase converts electrons from photoexcited CdS NRs into H₂ with high efficiency at this molar ratio. These results highlight the point that the key to fundamentally improving the photochemical activity of CdS–[FeFe] H₂ase complexes lies in increasing ϕ_{ET} . Increasing the electron-injection rate $\nu_{\text{ex}}\phi_{\text{ET}}$ is only beneficial for the TOF until it matches the rates of intraprotein charge transport or catalysis. At higher injection rates, electrons would be supplied faster than the enzyme can use them. This regime has not yet been observed in NC–H₂ase complexes.

While the rate of catalysis may be diffusion-limited in redox-mediated systems, the upper limit for the quantum yield of H₂ formation is still defined by ϕ_{ET} , as it is in bound NC–H₂ase complexes. However, the overall efficiency of ET in such systems is determined by the individual efficiencies of ET between the NC and the mediator as well as between the mediator and the enzyme (31), as described in Section 5.2. As a result, the greatest quantum yield of H₂ production in CdSe–[NiFe] H₂ase was achieved by selection of a mediator redox potential that balanced both ET steps to maximize the overall ϕ_{ET} (31).

In multielectron photochemistry, cocatalysts must accumulate multiple charges on a timescale shorter than the lifetime of the reaction intermediate to complete a catalytic cycle. Thus, while adding more cocatalysts to a particular donor increases ϕ_{ET} (Equation 2), the efficiency of the multielectron reaction can suffer if back-ET can occur because the cocatalysts compete with each other for sequentially photoexcited charge carriers (117). Even very slow and inefficient back-ET will have this effect when the time between excitations is relatively long (on the order of milliseconds), giving ample time for cocatalysts to lose some of their accumulated charges. This effect was observed in the CdS–H₂ase system, which exhibits a maximum efficiency of H₂ production at H₂ase:NC molar ratios near 1:1 (16). H₂ production is only a two-electron reaction, and this behavior may become more pronounced for reactions that require more electrons (117), such as N₂ fixation (25). Enzymes may outperform traditional synthetic cocatalysts in this regard, because

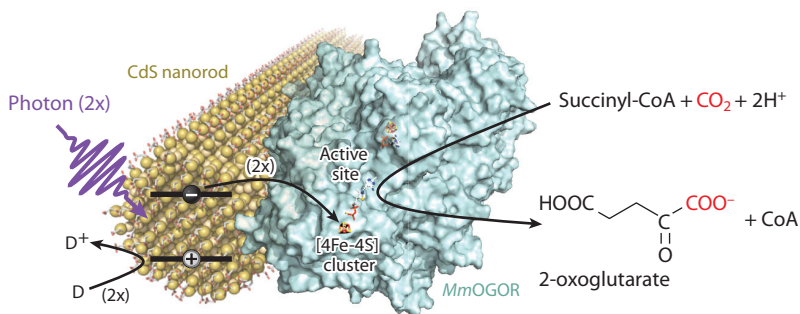


Figure 7

Light-driven C–C bond formation via CO₂ reduction by complexes of CdS NRs and the *Mm*OGOR enzyme. Photoexcited electrons are transferred from CdS to *Mm*OGOR, where CO₂ and succinyl-CoA are converted into 2-oxoglutarate and CoA while an electron donor (D) scavenges the photoexcited holes from CdS. Figure modified with permission from Reference 24; copyright 2020 National Academy of Sciences. Abbreviations: CoA, coenzyme A; *Mm*OGOR, 2-oxoglutarate:ferredoxin oxidoreductase from *Magnetococcus marinus*.

NC–enzyme systems feature large charge-separation distances, multistep electron transport, and relatively stable reaction intermediates (20).

7. NANOCRYSTAL–ENZYME ELECTRON TRANSFER FOR PHOTOCHEMICAL CARBON–CARBON BOND FORMATION

Enzymatic catalysis is particularly intriguing when it yields products that are difficult to synthesize cost-effectively by artificial means, such as transportation fuels, fertilizer, and other value-added compounds (2, 4, 25). As noted in Section 1, NC–enzyme architectures have expanded beyond H₂ production to drive a variety of multielectron reactions. Coupling light-absorbing NCs with increasingly complex enzymatic reactions introduces new potential considerations, such as an increase in the number of sequential ET steps, reaction intermediate instability, side reactions and products, and enzyme conformational complexity. However, little is known about the kinetics of ET from the NC to the enzyme in these more complex systems. Here, we review the insights reported in a recent study of an NC–enzyme system for light-driven C–C bond formation via CO₂ reduction (24).

2-Oxoglutarate:ferredoxin oxidoreductase from *Magnetococcus marinus* (*Mm*OGOR) is a dimeric enzyme that forms C–C bonds through conversion of CO₂ and succinyl-coenzyme A (succinyl-CoA) to 2-oxoglutarate and CoA (118). This reaction—proceeding via multiple intermediates and two electron injections to the enzyme—forms one stage of the reverse (reductive) tricarboxylic acid cycle used by some bacteria (119). Analogous to the NC–H₂ase systems described above, CdS NRs were used to provide the photoexcited electrons to drive the enzyme catalysis (24) (**Figure 7**). However, unlike H₂ase, *Mm*OGOR undergoes substantial conformational changes over the course of catalysis, which have been shown to strongly impact the NC–enzyme binding and, consequently, ET (24).

While the maximum product formation rates from the light-driven CdS–*Mm*OGOR system were comparable to the in vivo ferredoxin-driven reaction (120), the quantum efficiency of product formation was quite low (around 1%) when compared to the H₂ase systems (16, 24). The value of k_{ET} from CdS to *Mm*OGOR, obtained by TA spectroscopy, was of comparable magnitude to

that seen in CdS–H₂ase systems. However, upon addition of succinyl-CoA substrate, the ET efficiency decreased drastically. This decreased efficiency was attributed to conformational changes that *Mm*OGOR undergoes upon the binding of succinyl-CoA (120), which resulted in weaker NC–enzyme binding. Moreover, because *Mm*OGOR is a dimeric enzyme, the binding interaction of CdS NRs is stronger with the enzyme subunit that does not have succinyl-CoA bound and is therefore not poised for catalysis. This competition for electrons contributes to the low overall photochemical efficiency. As a result, the conditions required for enzyme catalysis (in this case, substrate binding) decrease the efficiency of electron injection into the enzyme (24). This example illustrates that increasing catalytic complexity and conformational changes introduced by large molecular substrates may require new levels of tunability and control to enable efficient light-driven catalysis.

8. SUMMARY AND OUTLOOK

In this article, we have reviewed the strategies for assembling semiconductor NCs and redox enzymes to drive multielectron chemistry with light, described spectroscopic measurements of the kinetics of ET from NCs to enzymes, discussed the factors that govern these kinetics, and summarized what is known about the fate of electrons transferred from NCs into H₂ases. Electron injection from photoexcited NCs to enzymes has been achieved in bound complexes, as well as systems where redox mediators shuttle electrons between the NC and the enzyme. These photoexcited electrons have participated in a wide range of multielectron redox reactions. The use of photoexcited NCs as sensitizers for redox enzymes also opens a new avenue for mechanistic studies of the enzymes themselves. For the prototypical systems that combine NCs with H₂ases, ET kinetics have been mapped out and discussed within the framework of Marcus theory.

Progress made thus far in systems that combine Cd-chalcogenide NCs with H₂ases has laid the foundation for the understanding of binding interactions and photoinduced charge transfer between NCs and redox enzymes. However, more work is needed to further our fundamental understanding of these biohybrid systems and extend those principles to the development of new architectures for light-driven chemistry. The ET step that has been the focus of this review is only one of several chemical steps involved in the photochemistry of NC–enzyme complexes. There has been some progress in understanding the factors that control k_{ET} within the framework of Marcus theory, but challenges remain in disentangling the Marcus parameters from geometric and binding considerations. The extent of coupling between ET and proton-transfer steps also remains to be determined (21). Additionally, measurements performed thus far have only probed the first ET step from the NC to the enzyme. It has been proposed that the second electron used in H₂ formation transfers with the same kinetics because the first electron transferred is transported to the active site buried far inside the enzyme, and the ET kinetics are thought to be determined by the interface between the NC and the first accessory cluster in the enzyme (20). However, this may not necessarily be the case in other NC–enzyme systems where the active site catalysis may be more closely coupled to the ET interface (24).

In addition to ET from the NC to the enzyme, other critical chemical steps are also not well understood. Perhaps most glaring is the sacrificial scavenging of photoexcited holes from NCs. Few electron acceptors normally used with NCs are compatible with enzymes; those that have been used in NC–H₂ase systems (i.e., ascorbate, cysteine, glutathione, and mercaptopropionic acid) are inefficient, requiring large excesses in solution and occasionally limiting sample stability (5, 16, 28). Because of efficient hole trapping and weak spectroscopic signals, hole dynamics are more difficult to study spectroscopically than electron dynamics in Cd-chalcogenide NCs (84, 88, 91, 94). While hole scavenging has been found to be the efficiency-limiting process in systems

where ET to the reduction catalyst is fast (e.g., CdS–Pt) (121, 122), its role in limiting the NC–enzyme systems remains to be determined. In addition to the questions about hole scavenging, much remains to be learned about how to control the binding interactions between NCs and enzymes, as well as the fate of the electrons that transfer to the enzyme.

Finally, arguably the most important remaining question is how the principles learned from NC–H₂ase systems can be applied to drive a wide range of enzymatic reactions with light. There has already been rapid growth in the variety of photochemical reactions carried out by NC–enzyme systems, including difficult reactions such as C–C bond formation (24), N₂ fixation (25), stereoselective chemistry (18), and targeted photooxidation reactions for sensing applications (11–13, 15, 27, 29). As the example of the CdS–*Mm*OGOR system illustrates, electron injection from an NC to the enzyme may be more intricate when the enzyme catalysis involves large substrates and structural rearrangements (24). Photoexcited NCs have also even been investigated for driving intracellular synthesis, sidestepping the need for enzyme extraction and opening the door to an even greater range of possible chemistries (123–126). The limits of reaction complexity attainable by biohybrid systems are not yet in sight. Our optimistic assessment is that the tunability in electronic structure, geometry, and surface chemistry that NCs provide will enable future strides in light-driven chemistry.

SUMMARY POINTS

1. Nanocrystal (NC)–enzyme hybrid structures integrate the tunable electronic structure, size, and surface chemistry of NCs with the remarkable catalytic properties of enzymes.
2. NC–enzyme systems have been shown to perform multielectron photochemistry, including reduction of protons, N₂, CO₂, fumarate, nitrate, aldehydes, and NADP⁺, as well as oxidation of sugars, lactate, sulfite, myristic acid, and superoxide.
3. Electron transfer (ET) from NCs to enzymes plays a key role in the photochemical activity of NC–enzyme systems.
4. ET between NCs and enzymes can occur directly in bound complexes or via a redox mediator.
5. The rate constant of ET has been measured using time-resolved spectroscopy and kinetic modeling.
6. The factors that control ET rates in NC–enzyme complexes have been described within the framework of Marcus theory for nonadiabatic ET.
7. Intraprotein electron transport that follows ET has been probed, resulting in direct evidence for NC-to-enzyme ET, greater understanding of NC–enzyme binding orientation, and new methods for investigation of the mechanisms of enzyme catalysis.
8. Fundamental insights into how NC–enzyme systems work are needed to take advantage of the tunability offered by NCs.

DISCLOSURE STATEMENT

The authors are not aware of any affiliations, memberships, funding, or financial holdings that might be perceived as affecting the objectivity of this review.

ACKNOWLEDGMENTS

The writing of this review was supported by the US Department of Energy, Office of Science, Basic Energy Sciences, under award DE-SC0010334 as well as the US Department of Energy, Office of Science, Basic Energy Sciences, Chemical Sciences, Geosciences and Biosciences Division through the National Renewable Energy Laboratory under contract DE-AC36-08GO28308. We gratefully acknowledge our collaborators in this research area: Paul King, Kate Brown, David Mulder, Sean Elliott, Joel Eaves, Lance Seefeldt, John Peters, and their coworkers.

LITERATURE CITED

1. Woolerton TW, Sheard S, Chaudhary YS, Armstrong FA. 2012. Enzymes and bio-inspired electrocatalysts in solar fuel devices. *Energy Environ. Sci.* 5(6):7470–90
2. Evans RM, Siritanaratkul B, Megarity CF, Pandey K, Esterle TF, et al. 2019. The value of enzymes in solar fuels research—efficient electrocatalysts through evolution. *Chem. Soc. Rev.* 48(7):2039–52
3. King PW. 2013. Designing interfaces of hydrogenase-nanomaterial hybrids for efficient solar conversion. *Biochim. Biophys. Acta* 1827(8–9):949–57
4. Lee SH, Choi DS, Kuk SK, Park CB. 2018. Photobiocatalysis: activating redox enzymes by direct or indirect transfer of photoinduced electrons. *Angew. Chem. Int. Ed.* 57(27):7958–85
5. Greene BL, Vansuch GE, Chica BC, Adams MWW, Dyer RB. 2017. Applications of photogating and time resolved spectroscopy to mechanistic studies of hydrogenases. *Acc. Chem. Res.* 50(11):2718–26
6. Alberty WJ, Knowles JR. 1976. Evolution of enzyme function and development of catalytic efficiency. *Biochemistry* 15(25):5631–40
7. Lewis K. 1966. Symposium on bioelectrochemistry of microorganisms. IV. Biochemical fuel cells. *Bacteriol. Rev.* 30(1):101–13
8. Parkinson BA, Weaver PF. 1984. Photoelectrochemical pumping of enzymatic CO₂ reduction. *Nature* 309(5964):148–49
9. Lubner CE, Grimme R, Bryant DA, Golbeck JH. 2010. Wiring Photosystem I for direct solar hydrogen production. *Biochemistry* 49(3):404–14
10. Kornienko N, Zhang JZ, Sakimoto KK, Yang PD, Reisner E. 2018. Interfacing nature's catalytic machinery with synthetic materials for semi-artificial photosynthesis. *Nat. Nanotechnol.* 13(10):890–99
11. Ipe BI, Niemeyer CM. 2006. Nanohybrids composed of quantum dots and cytochrome P450 as photocatalysts. *Angew. Chem. Int. Ed.* 45(3):504–7
12. Katz E, Zayats M, Willner I, Lisdat F. 2006. Controlling the direction of photocurrents by means of CdS nanoparticles and cytochrome *c*-mediated biocatalytic cascades. *Chem. Commun.* 2006(13):1395–97
13. Stoll C, Gehring C, Schubert K, Zanella M, Parak WJ, Lisdat F. 2008. Photoelectrochemical signal chain based on quantum dots on gold—sensitive to superoxide radicals in solution. *Biosens. Bioelectron.* 24(2):260–65
14. Brown KA, Dayal S, Ai X, Rumbles G, King PW. 2010. Controlled assembly of hydrogenase-CdTe nanocrystal hybrids for solar hydrogen production. *J. Am. Chem. Soc.* 132(28):9672–80
15. Schubert K, Khalid W, Yue Z, Parak WJ, Lisdat F. 2010. Quantum-dot-modified electrode in combination with NADH-dependent dehydrogenase reactions for substrate analysis. *Langmuir* 26(2):1395–400
16. Brown KA, Wilker MB, Boehm M, Dukovic G, King PW. 2012. Characterization of photochemical processes for H₂ production by CdS nanorod-[FeFe] hydrogenase complexes. *J. Am. Chem. Soc.* 134(12):5627–36
17. Greene BL, Joseph CA, Maroney MJ, Dyer RB. 2012. Direct evidence of active-site reduction and photodriven catalysis in sensitized hydrogenase assemblies. *J. Am. Chem. Soc.* 134:11108–11
18. Burai TN, Panay AJ, Zhu HM, Lian TQ, Lutz S. 2012. Light-driven, quantum dot-mediated regeneration of FMN to drive reduction of ketoisophorone by old yellow enzyme. *ACS Catal.* 2(4):667–70
19. Chaudhary YS, Woolerton TW, Allen CS, Warner JH, Pierce E, et al. 2012. Visible light-driven CO₂ reduction by enzyme coupled CdS nanocrystals. *Chem. Commun.* 48(1):58–60

20. Wilker MB, Shinopoulos KE, Brown KA, Mulder DW, King PW, Dukovic G. 2014. Electron transfer kinetics in CdS nanorod-[FeFe]-hydrogenase complexes and implications for photochemical H₂ generation. *J. Am. Chem. Soc.* 136(11):4316–24
21. Brown KA, Song Q, Mulder DW, King PW. 2014. Diameter dependent electron transfer kinetics in semiconductor-enzyme complexes. *ACS Nano* 8(10):10790–98
22. Utterback JK, Wilker MB, Brown KA, King PW, Eaves JD, Dukovic G. 2015. Competition between electron transfer, trapping, and recombination in CdS nanorod-hydrogenase complexes. *Phys. Chem. Chem. Phys.* 17(8):5538–42
23. Sabir N, Khan N, Volkner J, Widdascheck F, del Pino P, et al. 2015. Photo-electrochemical bioanalysis of guanosine monophosphate using coupled enzymatic reactions at a CdS/ZnS quantum dot electrode. *Small* 11(43):5844–50
24. Hamby H, Li B, Shinopoulos KE, Keller HR, Elliott SJ, Dukovic G. 2020. Light-driven carbon-carbon bond formation via CO₂ reduction catalyzed by complexes of CdS nanorods and a 2-oxoacid oxidoreductase. *PNAS* 117(1): 135–40
25. Brown KA, Harris DF, Wilker MB, Rasmussen A, Khadka N, et al. 2016. Light-driven dinitrogen reduction catalyzed by a CdS:nitrogenase MoFe protein biohybrid. *Science* 352(6284):448–50
26. Brown KA, Wilker MB, Boehm M, Hamby H, Dukovic G, King PW. 2016. Photocatalytic regeneration of nicotinamide cofactors by quantum dot-enzyme biohybrid complexes. *ACS Catal.* 6(4):2201–4
27. Zeng T, Leimkuhler S, Koetz J, Wollenberger U. 2015. Effective electrochemistry of human sulfite oxidase immobilized on quantum-dots-modified indium tin oxide electrode. *ACS Appl. Mater. Interfaces* 7(38):21487–94
28. Chica B, Wu CH, Liu Y, Adams MWW, Lian TQ, Dyer RB. 2017. Balancing electron transfer rate and driving force for efficient photocatalytic hydrogen production in CdSe/CdS nanorod-[NiFe] hydrogenase assemblies. *Energy Environ. Sci.* 10(10):2245–55
29. Riedel M, Sabir N, Scheller FW, Parak WJ, Lisdat F. 2017. Connecting quantum dots with enzymes: mediator-based approaches for the light-directed read-out of glucose and fructose oxidation. *Nanoscale* 9(8):2814–23
30. Wilker MB, Utterback JK, Greene S, Brown KA, Mulder DW, et al. 2018. Role of surface-capping ligands in photoexcited electron transfer between CdS nanorods and [FeFe] hydrogenase and the subsequent H₂ generation. *J. Phys. Chem. C* 122(1):741–50
31. Sanchez MLK, Wu CH, Adams MWW, Dyer RB. 2019. Optimizing electron transfer from CdSe QDs to hydrogenase for photocatalytic H₂ production. *Chem. Commun.* 55(39):5579–82
32. Utterback JK, Wilker MB, Mulder DW, King PW, Eaves JD, Dukovic G. 2019. Quantum efficiency of charge transfer competing against nonexponential processes: the case of electron transfer from CdS nanorods to hydrogenase. *J. Phys. Chem. C* 123(1):886–96
33. Riedel M, Parak WJ, Ruff A, Schuhmann W, Lisdat F. 2018. Light as trigger for biocatalysis: photonic wiring of flavin adenine dinucleotide-dependent glucose dehydrogenase to quantum dot-sensitized inverse opal TiO₂ architectures via redox polymers. *ACS Catal.* 8(6):5212–20
34. Hutton GAM, Reuillard B, Martindale BCM, Caputo CA, Lockwood CWJ, et al. 2016. Carbon dots as versatile photosensitizers for solar-driven catalysis with redox enzymes. *J. Am. Chem. Soc.* 138(51):16722–30
35. Kim J, Lee SH, Tieves F, Choi DS, Hollmann F, et al. 2018. Biocatalytic C=C bond reduction through carbon nanodot-sensitized regeneration of NADH analogues. *Angew. Chem. Int. Ed.* 57(42):13825–28
36. Liu J, Huang JH, Zhou H, Antonietti M. 2014. Uniform graphitic carbon nitride nanorod for efficient photocatalytic hydrogen evolution and sustained photoenzymatic catalysis. *ACS Appl. Mater. Interfaces* 6(11):8434–40
37. Selvaggi A, Tosi C, Barberini U, Franchi E, Rodriguez F, Pedroni P. 1999. In vitro hydrogen photoproduction using *Pyrococcus furiosus* sulfhydrogenase and TiO₂. *J. Photochem. Photobiol.* 125(1–3):107–12
38. Reisner E, Fontecilla-Camps JC, Armstrong FA. 2009. Catalytic electrochemistry of a [NiFeSe]-hydrogenase on TiO₂ and demonstration of its suitability for visible-light driven H₂ production. *Chem. Commun.* 2009(5):550–52

39. Reisner E, Powell DJ, Cavazza C, Fontecilla-Camps JC, Armstrong FA. 2009. Visible light-driven H₂ production by hydrogenases attached to dye-sensitized TiO₂ nanoparticles. *J. Am. Chem. Soc.* 131(51):18457–66
40. Woolerton TW, Sheard S, Reisner E, Pierce E, Ragsdale SW, Armstrong FA. 2010. Efficient and clean photoreduction of CO₂ to CO by enzyme-modified TiO₂ nanoparticles using visible light. *J. Am. Chem. Soc.* 132(7):2132–33
41. Mifsud M, Gargiulo S, Iborra S, Arends IWCE, Hollmann F, Corma A. 2014. Photobiocatalytic chemistry of oxidoreductases using water as the electron donor. *Nat. Commun.* 5:3145
42. Caputo CA, Wang LD, Beranek R, Reisner E. 2015. Carbon nitride-TiO₂ hybrid modified with hydrogenase for visible light driven hydrogen production. *Chem. Sci.* 6(10):5690–94
43. Siritanaratkul B, Islam STA, Schubert T, Kunze C, Goris T, et al. 2016. Selective, light-driven enzymatic dehalogenations of organic compounds. *RSC Adv.* 6(88):84882–86
44. Zhang LY, Can M, Ragsdale SW, Armstrong FA. 2018. Fast and selective photoreduction of CO₂ to CO catalyzed by a complex of carbon monoxide dehydrogenase, TiO₂, and Ag nanoclusters. *ACS Catal.* 8(4):2789–95
45. Allakhverdiev SI, Kreslavski VD, Thavasi V, Zharmukhamedov SK, Klimov VV, et al. 2009. Hydrogen photoproduction by use of photosynthetic organisms and biomimetic systems. *Photochem. Photobiol. Sci.* 8(2):148–56
46. Hambourger M, Kodis G, Vaughn MD, Moore GF, Gust D, et al. 2009. Solar energy conversion in a photoelectrochemical biofuel cell. *Dalton Trans.* 2009(45):9979–89
47. Reisner E. 2011. Solar hydrogen evolution with hydrogenases: from natural to hybrid systems. *Eur. J. Inorg. Chem.* 2011(7):1005–16
48. Tran PD, Barber J. 2012. Proton reduction to hydrogen in biological and chemical systems. *Phys. Chem. Chem. Phys.* 14(40):13772–84
49. Tran PD, Wong LH, Barber J, Loo JSC. 2012. Recent advances in hybrid photocatalysts for solar fuel production. *Energy Environ. Sci.* 5(3):5902–18
50. Wilker MB, Schnitzenbaumer KJ, Dukovic G. 2012. Recent progress in photocatalysis mediated by colloidal II–VI nanocrystals. *Isr. J. Chem.* 52(11–12):1002–15
51. Zadovorny OA, Lucon JE, Gerlach R, Zorin NA, Douglas T, et al. 2012. Photo-induced H₂ production by [NiFe]-hydrogenase from *T. roseopersicina* covalently linked to a Ru(II) photosensitizer. *J. Inorg. Biochem.* 106(1):151–55
52. Lee SH, Ryu J, Nam DH, Park CB. 2011. Photoenzymatic synthesis through sustainable NADH regeneration by SiO₂-supported quantum dots. *Chem. Commun.* 47(16):4643–45
53. Yu WW, Qu L, Guo W, Peng X. 2003. Experimental determination of the extinction coefficient of CdTe, CdSe, and CdS nanocrystals. *Chem. Mater.* 15(14):2854–60
54. Burda C, Chen XB, Narayanan R, El-Sayed MA. 2005. Chemistry and properties of nanocrystals of different shapes. *Chem. Rev.* 105(4):1025–102
55. Knowles KE, Peterson MD, McPhail MR, Weiss EA. 2013. Exciton dissociation within quantum dot-organic complexes: mechanisms, use as a probe of interfacial structure, and applications. *J. Phys. Chem. C* 117(20):10229–43
56. Bawendi MG, Steigerwald ML, Brus LE. 1990. The quantum mechanics of larger semiconductor clusters (“quantum dots”). *Annu. Rev. Phys. Chem.* 41:477–96
57. Peng XG, Manna L, Yang WD, Wickham J, Scher E, et al. 2000. Shape control of CdSe nanocrystals. *Nature* 404(6773):59–61
58. Peterson MD, Cass LC, Harris RD, Edme K, Sung K, Weiss EA. 2014. The role of ligands in determining the exciton relaxation dynamics in semiconductor quantum dots. *Annu. Rev. Phys. Chem.* 65:317–39
59. Zhu HM, Song NH, Lian TQ. 2010. Controlling charge separation and recombination rates in CdSe/ZnS type I core-shell quantum dots by shell thicknesses. *J. Am. Chem. Soc.* 132(42):15038–45
60. Tisdale WA, Zhu XY. 2011. Artificial atoms on semiconductor surfaces. *PNAS* 108(3):965–70
61. Xiong W, Hickstein DD, Schnitzenbaumer KJ, Ellis JL, Palm BB, et al. 2013. Photoelectron spectroscopy of CdSe nanocrystals in the gas phase: a direct measure of the evanescent electron wave function of quantum dots. *Nano Lett.* 13(6):2924–30

62. Ekimov AI, Onushchenko AA. 1981. Quantum size effect in three-dimensional microscopic semiconductor crystals. *J. Exp. Theor. Phys. Lett.* 34:345–49
63. Vincent KA, Parkin A, Armstrong FA. 2007. Investigating and exploiting the electrocatalytic properties of hydrogenases. *Chem. Rev.* 107(10):4366–413
64. Ratzloff MW, Wilker MB, Mulder DW, Lubner CE, Hamby H, et al. 2017. Activation thermodynamics and H/D kinetic isotope effect of the H_{ox} to H_{red}H⁺ transition in [FeFe] hydrogenase. *J. Am. Chem. Soc.* 139(37):12879–82
65. Macia-Agullo JA, Corma A, Garcia H. 2015. Photobiocatalysis: the power of combining photocatalysis and enzymes. *Chem. Eur. J.* 21(31):10940–59
66. Hutton GAM, Martindale BCM, Reisner E. 2017. Carbon dots as photosensitisers for solar-driven catalysis. *Chem. Soc. Rev.* 46(20):6111–23
67. Sakimoto KK, Kornienko N, Cestellos-Blanco S, Lim J, Liu C, Yang PD. 2018. Physical biology of the materials-microorganism interface. *J. Am. Chem. Soc.* 140(6):1978–85
68. Valentine RC. 1964. Bacterial ferredoxin. *Bacteriol. Rev.* 28(4):497–517
69. Piculle L, Nouailler M, Morelli X, Cavazza C, Gallice P, et al. 2004. Multiple orientations in a physiological complex: the pyruvate-ferredoxin oxidoreductase-ferredoxin system. *Biochemistry* 43(49):15480–93
70. Demuez M, Cournac L, Guerrini O, Soucaille P, Girbal L. 2007. Complete activity profile of *Clostridium acetobutylicum* [FeFe]-hydrogenase and kinetic parameters for endogenous redox partners. *FEMS Microbiol. Lett.* 275(1):113–21
71. Long H, Chang CH, King PW, Ghirardi ML, Kim K. 2008. Brownian dynamics and molecular dynamics study of the association between hydrogenase and ferredoxin from *Chlamydomonas reinhardtii*. *Biophys. J.* 95(8):3753–66
72. Hamon C, Ciaccavava A, Infossi P, Puppo R, Even-Hernandez P, et al. 2014. Synthesis and enzymatic photo-activity of an O₂ tolerant hydrogenase–CdSe@CdS quantum rod bioconjugate. *Chem. Commun.* 50(39):4989–92
73. Zhang LY, Beaton SE, Carr SB, Armstrong FA. 2018. Direct visible light activation of a surface cysteine-engineered [NiFe]-hydrogenase by silver nanoclusters. *Energy Environ. Sci.* 11(12):3342–48
74. Ding TX, Olshansky JH, Leone SR, Alivisatos AP. 2015. Efficiency of hole transfer from photoexcited quantum dots to covalently linked molecular species. *J. Am. Chem. Soc.* 137(5):2021–29
75. Tachiya M. 1975. Application of a generating function to reaction-kinetics in micelles: kinetics of quenching of luminescent probes in micelles. *Chem. Phys. Lett.* 33(2):289–92
76. Tachiya M. 1982. Kinetics of quenching of luminescent probes in micellar systems. II. *J. Phys. Chem.* 76(1):340–48
77. Sadhu S, Tachiya M, Patra A. 2009. A stochastic model for energy transfer from CdS quantum dots/rods (donors) to Nile Red dye (acceptors). *J. Phys. Chem. C* 113(45):19488–92
78. Song NH, Zhu HM, Jin SY, Zhan W, Lian TQ. 2011. Poisson-distributed electron-transfer dynamics from single quantum dots to C60 molecules. *ACS Nano* 5(1):613–21
79. Morris-Cohen AJ, Frederick MT, Cass LC, Weiss EA. 2011. Simultaneous determination of the adsorption constant and the photoinduced electron transfer rate for a CdS quantum dot-viologen complex. *J. Am. Chem. Soc.* 133(26):10146–54
80. Morris-Cohen AJ, Vasilenko V, Amin VA, Reuter MG, Weiss EA. 2012. Model for adsorption of ligands to colloidal quantum dots with concentration-dependent surface structure. *ACS Nano* 6(1):557–65
81. Anderson NA, Lian TQ. 2005. Ultrafast electron transfer at the molecule-semiconductor nanoparticle interface. *Annu. Rev. Phys. Chem.* 56:491–519
82. McArthur EA, Morris-Cohen AJ, Knowles KE, Weiss EA. 2010. Charge carrier resolved relaxation of the first excitonic state in CdSe quantum dots probed with near-infrared transient absorption spectroscopy. *J. Phys. Chem. B* 114(45):14514–20
83. Tvrđy K, Frantsuzov PA, Kamat PV. 2011. Photoinduced electron transfer from semiconductor quantum dots to metal oxide nanoparticles. *PNAS* 108(1):29–34
84. Wu K, Zhu H, Liu Z, Rodriguez-Cordoba W, Lian T. 2012. Ultrafast charge separation and long-lived charge separated state in photocatalytic CdS–Pt nanorod heterostructures. *J. Am. Chem. Soc.* 134(25):10337–40

85. Baxter JB, Richter C, Schmuttenmaer CA. 2014. Ultrafast carrier dynamics in nanostructures for solar fuels. *Annu. Rev. Phys. Chem.* 65:423–47
86. Wu KF, Lian TQ. 2016. Quantum confined colloidal nanorod heterostructures for solar-to-fuel conversion. *Chem. Soc. Rev.* 45(14):3781–810
87. Zhu HM, Yang Y, Wu KF, Lian TQ. 2016. Charge transfer dynamics from photoexcited semiconductor quantum dots. *Annu. Rev. Phys. Chem.* 67:259–81
88. Klimov VI. 2007. Spectral and dynamical properties of multiexcitons in semiconductor nanocrystals. *Annu. Rev. Phys. Chem.* 58:635–73
89. Nozik AJ, Beard MC, Luther JM, Law M, Ellingson RJ, Johnson JC. 2010. Semiconductor quantum dots and quantum dot arrays and applications of multiple exciton generation to third-generation photovoltaic solar cells. *Chem. Rev.* 110(11):6873–90
90. Zhu HM, Song NH, Lian TQ. 2011. Wave function engineering for ultrafast charge separation and slow charge recombination in type II core/shell quantum dots. *J. Am. Chem. Soc.* 133(22):8762–71
91. Grimaldi G, Geuchies JJ, van der Stam W, du Fossé I, Brynjarsson B, et al. 2019. Spectroscopic evidence for the contribution of holes to the bleach of Cd-chalcogenide quantum dots. *Nano Lett.* 19(5):3002–10
92. Jones M, Scholes GD. 2010. On the use of time-resolved photoluminescence as a probe of nanocrystal photoexcitation dynamics. *J. Mater. Chem.* 20(18):3533–38
93. Knowles KE, McArthur EA, Weiss EA. 2011. A multi-timescale map of radiative and nonradiative decay pathways for excitons in CdSe quantum dots. *ACS Nano* 5(3):2026–35
94. Utterback JK, Grennell AN, Wilker MB, Pearce O, Eaves JD, Dukovic G. 2016. Observation of trapped-hole diffusion on the surfaces of CdS nanorods. *Nat. Chem.* 8(11):1061–66
95. Lakowicz JR. 2006. *Principles of Fluorescence Spectroscopy*. New York: Springer
96. Berberan-Santos MN, Bodunov EN, Valeur B. 2005. Mathematical functions for the analysis of luminescence decays with underlying distributions I. Kohlrausch decay function (stretched exponential). *Chem. Phys.* 315(1–2):171–82
97. Aldeek F, Safi M, Zhan NQ, Palui G, Mattoussi H. 2013. Understanding the self-assembly of proteins onto gold nanoparticles and quantum dots driven by metal-histidine coordination. *ACS Nano* 7(11):10197–210
98. Peterson MD, Jensen SC, Weinberg DJ, Weiss EA. 2014. Mechanisms for adsorption of methyl viologen on CdS quantum dots. *ACS Nano* 8(3):2826–37
99. Milton RD, Abdellaoui S, Khadka N, Dean DR, Leech D, et al. 2016. Nitrogenase bioelectrocatalysis: heterogeneous ammonia and hydrogen production by MoFe protein. *Energy Environ. Sci.* 9(8):2550–54
100. Marcus RA, Sutin N. 1985. Electron transfers in chemistry and biology. *Biochim. Biophys. Acta* 811(3):265–322
101. Newton MD. 1991. Quantum chemical probes of electron-transfer kinetics: the nature of donor-acceptor interactions. *Chem. Rev.* 91(5):767–92
102. Dibbell RS, Watson DF. 2009. Distance-dependent electron transfer in tethered assemblies of CdS quantum dots and TiO₂ nanoparticles. *J. Phys. Chem. C* 113(8):3139–49
103. Tagliazucchi M, Tice DB, Sweeney CM, Morris-Cohen AJ, Weiss EA. 2011. Ligand-controlled rates of photoinduced electron transfer in hybrid CdSe nanocrystal/poly(viologen) films. *ACS Nano* 5(12):9907–17
104. Hyun BR, Bartnik AC, Sun LF, Hanrath T, Wise FW. 2011. Control of electron transfer from lead-salt nanocrystals to TiO₂. *Nano Lett.* 11(5):2126–32
105. Wang H, McNellis ER, Kinge S, Bonn M, Canovas E. 2013. Tuning electron transfer rates through molecular bridges in quantum dot sensitized oxides. *Nano Lett.* 13(11):5311–15
106. Hines DA, Forrest RP, Corcelli SA, Kamat PV. 2015. Predicting the rate constant of electron tunneling reactions at the CdSe–TiO₂ interface. *J. Phys. Chem. B* 119(24):7439–46
107. Madden C, Vaughn MD, Díez-Pérez I, Brown KA, King PW, et al. 2012. Catalytic turnover of [FeFe]-hydrogenase based on single-molecule imaging. *J. Am. Chem. Soc.* 134(3):1577–82
108. Kroupa DM, Vörös M, Brawand NP, McNichols BW, Miller EM, et al. 2017. Tuning colloidal quantum dot band edge positions through solution-phase surface chemistry modification. *Nat. Commun.* 8:15257
109. Brown PR, Kim D, Lunt RR, Zhao N, Bawendi MG, et al. 2014. Energy level modification in lead sulfide quantum dot thin films through ligand exchange. *ACS Nano* 8(6):5863–72

110. Zhu HM, Yang Y, Hyeon-Deuk K, Califano M, Song NH, et al. 2014. Auger-assisted electron transfer from photoexcited semiconductor quantum dots. *Nano Lett.* 14(3):1263–69
111. Olshansky JH, Ding TX, Lee YV, Leone SR, Alivisatos AP. 2015. Hole transfer from photoexcited quantum dots: the relationship between driving force and rate. *J. Am. Chem. Soc.* 137(49):15567–75
112. Jones M, Lo SS, Scholes GD. 2009. Quantitative modeling of the role of surface traps in CdSe/CdS/ZnS nanocrystal photoluminescence decay dynamics. *PNAS* 106(9):3011–16
113. Tarafder K, Surendranath Y, Olshansky JH, Alivisatos AP, Wang LW. 2014. Hole transfer dynamics from a CdSe/CdS quantum rod to a tethered ferrocene derivative. *J. Am. Chem. Soc.* 136(13):5121–31
114. Moser CC, Keske JM, Warncke K, Farid RS, Dutton PL. 1992. Nature of biological electron transfer. *Nature* 355(6363):796–802
115. Gray HB, Winkler JR. 1996. Electron transfer in proteins. *Annu. Rev. Biochem.* 65:537–61
116. Mulder DW, Ratzloff MW, Shepard EM, Byer AS, Noone SM, et al. 2013. EPR and FTIR analysis of the mechanism of H₂ activation by [FeFe]-hydrogenase HydA1 from *Cblamydomonas reinhardtii*. *J. Am. Chem. Soc.* 135:6921–29
117. Nakibli Y, Kalisman P, Amirav L. 2015. Less is more: the case of metal cocatalysts. *J. Phys. Chem. Lett.* 6(12):2265–68
118. Williams TJ, Zhang CL, Scott JH, Bazylinski DA. 2006. Evidence for autotrophy via the reverse tricarboxylic acid cycle in the marine magnetotactic coccus strain MC-1. *Appl. Environ. Microbiol.* 72(2):1322–29
119. Fuchs G. 2011. Alternative pathways of carbon dioxide fixation: insights into the early evolution of life? *Annu. Rev. Microbiol.* 65:631–58
120. Chen PY-T, Li B, Drennan CL, Elliott SJ. 2019. A reverse TCA cycle 2-oxoacid:ferredoxin oxidoreductase that makes C-C bonds from CO₂. *Joule* 3(2):595–611
121. Wu K, Chen Z, Lv H, Zhu H, Hill CL, Lian T. 2014. Hole removal rate limits photodriven H₂ generation efficiency in CdS-Pt and CdSe/CdS-Pt semiconductor nanorod–metal tip heterostructures. *J. Am. Chem. Soc.* 136(21):7708–16
122. Berr MJ, Wagner P, Fischbach S, Vaneski A, Schneider J, et al. 2012. Hole scavenger redox potentials determine quantum efficiency and stability of Pt-decorated CdS nanorods for photocatalytic hydrogen generation. *Appl. Phys. Lett.* 100(22):223903
123. Sakimoto KK, Wong AB, Yang P. 2016. Self-photosensitization of nonphotosynthetic bacteria for solar-to-chemical production. *Science* 351(6268):74–77
124. Kornienko N, Sakimoto KK, Herlihy DM, Nguyen SC, Alivisatos AP, et al. 2016. Spectroscopic elucidation of energy transfer in hybrid inorganic–biological organisms for solar-to-chemical production. *PNAS* 113(42):11750–55
125. Ainsworth EV, Lockwood CWJ, White GF, Hwang ET, Sakai T, et al. 2016. Photoreduction of *Shewanella oneidensis* extracellular cytochromes by organic chromophores and dye-sensitized TiO₂. *Chem-BioChem* 17(24):2324–33
126. Honda Y, Watanabe M, Hagiwara H, Ida S, Ishihara T. 2017. Inorganic/whole-cell biohybrid photocatalyst for highly efficient hydrogen production from water. *Appl. Catal. B Environ.* 210:400–6